

ILC Extraction Line Simulations with TDR Parameters*

E. Marín and Y. Nosochkov
SLAC National Accelerator Laboratory, Menlo Park, CA 94025

Abstract

The goal of this study is to evaluate the impact of the latest ILC beam parameters at the Interaction Point (IP), as specified in the 2013 ILC Technical Design Report (TDR), on beam losses in the extraction line. The previous beam loss evaluation was based on the parameters specified in the 2007 ILC Reference Design Report (RDR). The results of this study are compared to the results obtained in the past for the “nominal” and the “low power” (low-P) parameter options of the RDR. The initial disrupted beam distribution at IP was generated using Guinea-Pig code, and the beam losses were obtained in tracking simulations using DIMAD. The study is performed for 500 GeV center-of-mass beam energy and the extraction line optics corresponding to the latest final focus optics with $L^* = 4.5$ m, with and without detector solenoid.

*Talk presented at the International Workshop on Future Linear Colliders (LCWS13)
Tokyo, Japan, 11-15 November 2013*

*Work supported by the US Department of Energy contract DE-AC02-76SF00515.

1 Introduction

The ILC extraction line [1] is designed for 14 mrad horizontal crossing angle at the Interaction Point (IP). The extraction optics provides large beam acceptance in order to minimize beam losses caused by long energy tail and large angular spread of the disrupted primary and secondary beams.

Previously, the extraction beam losses were evaluated [2] for the IP beam parameters specified in the 2007 ILC Reference Design Report (RDR) [3]. Recently, the updated beam parameters have been released in the 2013 ILC Technical Design Report (TDR) [4]. Therefore, it is important to verify the impact of the TDR parameters on the extraction losses.

The study is performed for 500 GeV center-of-mass beam energy and the extraction line optics [1] corresponding to the latest final focus (FF) optics with $L^* = 4.5$ m [5], with and without detector solenoid. The disrupted beam distribution at IP was generated using Guinea-Pig code [6], and the beam losses were evaluated in tracking simulations using DIMAD [7]. The results using the TDR parameters are compared with the results for the RDR “nominal” and “low power” (low-P) options as they have the parameters closest to the TDR ones.

2 Beam parameters

A beam collision, assuming the ILC parameters, will result in a strongly disrupted distribution of the electron beam having a long low energy tail and large angular spread. Trajectories of the low energy electrons are then further amplified by strong deflections ($\propto 1/E$) in the extraction line magnets which can lead to beam losses. The beam collision also creates a flux of beamstrahlung photons which can contribute to the total power loss.

In this study, the beam losses are determined by tracking the electron and photon beams from the IP to the extraction dump using DIMAD. The particles are considered lost when their trajectories exceed the size of the specified beam pipe aperture. The initial disrupted distributions of electrons and photons after collision were generated using Guinea-Pig code.

Tracking of $10^4 - 10^5$ electrons is typically sufficient for an estimate of beam properties after IP and for calculation of relatively high power loss in the extraction line collimators. However, an accurate estimate of much lower losses in magnets, which are mostly caused by low energy electrons, requires a higher statistics in the low energy tail corresponding to $10^6 - 10^7$ particles in the full beam. Tracking so many particles, however, takes much longer time and requires rather large storage space for the data. Fortunately, for this purpose it is not necessary to track the full beam because only electrons with very low energy and large IP $x - y$ angles are lost in the magnets. As a result, two types of beam data were used in this study. The low statistics data, typically containing $4 \cdot 10^4$ electrons in the full beam, were used for evaluation of beam distribution and calculation of high beam loss in the extraction collimators. The high statistics beams with about $4 \cdot 10^6$ electrons at IP were also generated, but only particles with energy below 70% of the nominal energy or x or y angles larger than 0.5 mrad at IP were used in tracking for calculating beam losses in magnets. The mentioned cuts reduce the beam population by a factor of 100.

The electron beam parameters for the TDR and the RDR nominal and low-P options are summarized in Table 1. Here, N_e is the number of electrons per bunch, N_b the number of bunches per pulse, f_{RF} the repetition rate, P the total beam power, $\beta_{x,y}^*$ the beta functions at IP, σ_z the bunch length, $\gamma\epsilon_{x,y}$ the normalized emittances, $D_{x,y}$ the disruption parameters, and δ_{BS} the fractional *rms* energy loss due to beamstrahlung.

A larger value of δ_{BS} indicates a longer low energy tail in the disrupted beam. Based on the

Table 1: Design electron beam parameters at IP in the TDR and the RDR nominal and low-P options.

	E GeV	N_e 10^{10}	N_b	f_{RF} Hz	P MW	β_x^* mm	β_y^* mm	σ_z mm	$\gamma\epsilon_x$ $\mu m \cdot rad$	$\gamma\epsilon_y$ $\mu m \cdot rad$	D_x	D_y	δ_{BS} %
TDR	250	2	1312	5	5.25	11	0.48	0.3	10	0.035	0.30	24.6	4.5
Nominal	250	2	2625	5	10.5	20	0.40	0.3	10	0.040	0.17	19.4	2.4
Low-P	250	2	1320	5	5.29	11	0.20	0.2	10	0.036	0.21	26.1	5.5

δ_{BS} values in Table 1 and taking into account that most of the electron losses occur in the low energy tail, it is expected that beam losses with the TDR beam parameters will be higher than in the RDR nominal option, but lower than in the low-P option.

2.1 Disrupted electron distribution at IP with the TDR parameters

The impact of beam disruption on electron beam size with the TDR parameters can be seen in Table 2. The values for the undisrupted beam correspond to the parameters in Table 1, and the values for disrupted beam are computed from the electron distribution generated by Guinea-Pig. One can see that the disruption effect significantly increases the transverse angular spread and the beam emittance. Fig. 1-3 show the x and y phase space, beam size and angular distributions for the disrupted beam with the TDR parameters. Note the sloped horizontal phase space in Fig. 1 and double peak horizontal angular spread in Fig. 3 characteristic for flat beam collisions.

Table 2: RMS beam size, beam angular divergence and emittance at IP with and without disruption for $4 \cdot 10^4$ electrons.

IP beam parameters	σ_x^* nm	σ_y^* nm	$\sigma_{x'}^*$ μrad	$\sigma_{y'}^*$ μrad	$\gamma\epsilon_x$ $\mu m \cdot rad$	$\gamma\epsilon_y$ $\mu m \cdot rad$
undisrupted	474	5.9	43	12.2	10	0.035
disrupted	493	9.9	284	36.2	36	0.164

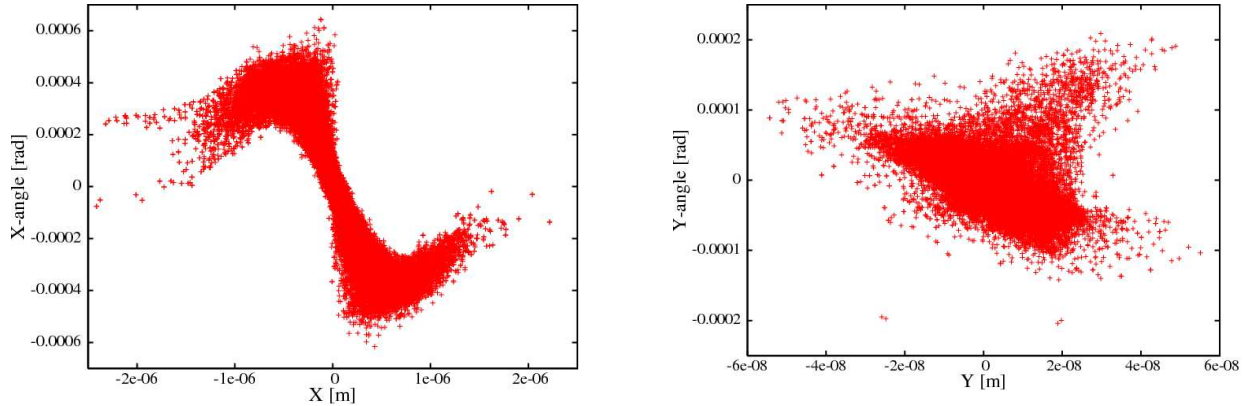


Figure 1: Disrupted beam phase space at IP with the TDR parameters for $4 \cdot 10^4$ electrons.

Fig. 4, 5 show the distribution of relative electron energy offsets $\Delta E/E$ in the disrupted beam with the TDR parameters. Electrons in the low energy tail will experience strong deflections ($\propto 1/E$) in the extraction magnets leading to large trajectories and potential loss on beam chamber.

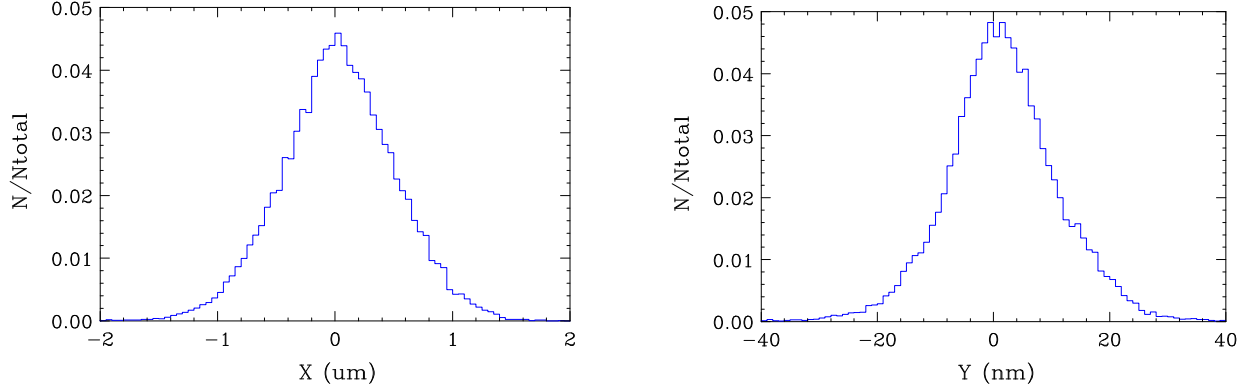


Figure 2: Disrupted horizontal (μm) and vertical (nm) distributions at IP with the TDR parameters for $4 \cdot 10^4$ electrons.

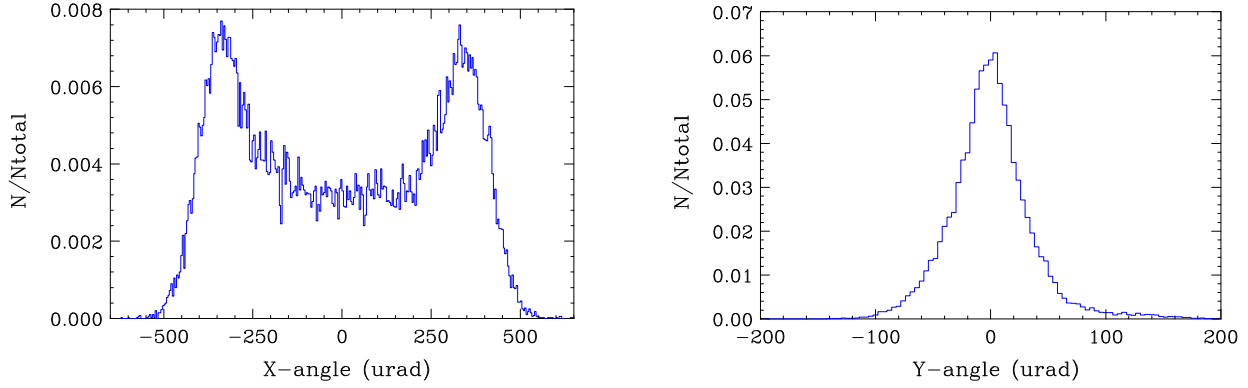


Figure 3: Disrupted angular distribution (μrad) at IP with the TDR parameters for $4 \cdot 10^4$ electrons.

The low electron energy and large IP angles are the main sources for the electron loss in the extraction magnets.

2.2 Beamstrahlung photon distribution at IP with the TDR parameters

Bending of the electron orbits in collision due to beam-beam forces results in radiation creating a flux of beamstrahlung photons traveling in the same direction with the primary electrons. The photons are not affected by the magnetic field of the extraction magnets, therefore their trajectories are determined strictly by the IP angles. Beam power in the beamstrahlung photon beam is not negligible, therefore the extraction line must provide sufficient aperture increasing with distance. The current design has the magnet aperture accommodating photon angles up to ± 0.75 mrad.

Table 3 shows *rms* and maximum photon angles with the TDR parameters for $3.6 \cdot 10^4$ photons generated by Guinea-Pig. Note that this angular spread is well within the extraction magnet aperture, although larger angles can occur if a higher statistics is generated or other mechanisms are considered (e.g. non-ideal collisions). The beamstrahlung angular x and y distributions at IP with the TDR parameters are shown in Fig. 6.

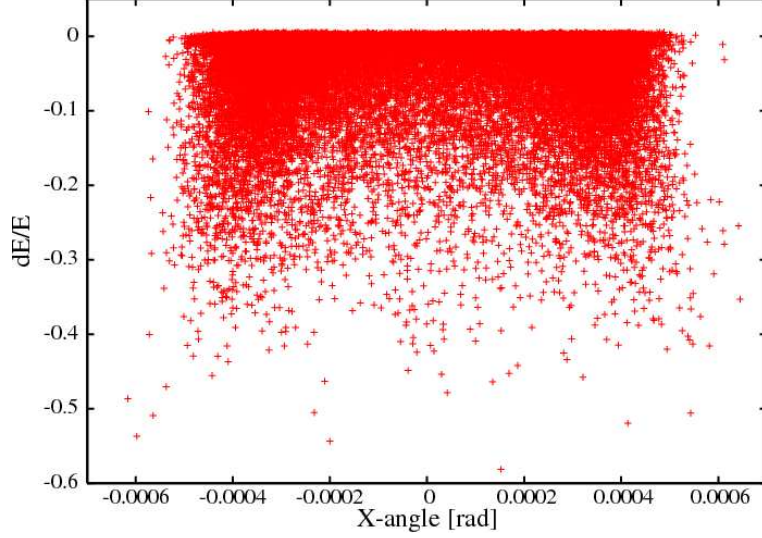


Figure 4: Disrupted $\Delta E/E$ versus horizontal angle at IP with the TDR parameters for $4 \cdot 10^4$ electrons.

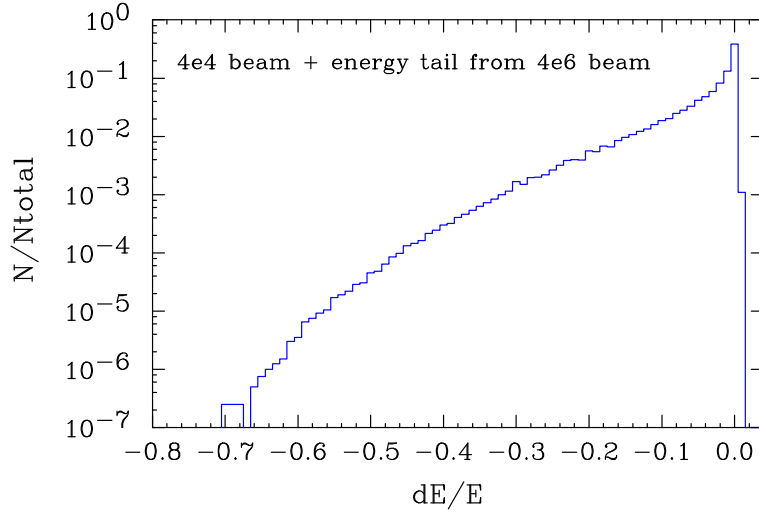


Figure 5: Disrupted energy distribution at IP with the TDR parameters for $4 \cdot 10^6$ electrons.

Table 3: RMS divergence and maximum angles at IP for beam of $3.6 \cdot 10^4$ beamstrahlung photons.

$\sigma_{x'}^*$	$\sigma_{y'}^*$	x'_{max}	y'_{max}
184 μrad	47 μrad	559 μrad	308 μrad

3 Extraction line optics

Detailed description of the extraction line optics can be found in [1]. The design accommodates a range of L^* in the FF from 3.5 m to 4.5 m. In this study, the FF optics with $L^* = 4.5$ m [5] is used. The corresponding extraction optics has a free space $L_{ext}^* = 6.3$ m between IP and the nearest extraction quadrupole.

The extraction line layout and optics functions for the TDR parameters are shown in Fig. 7.

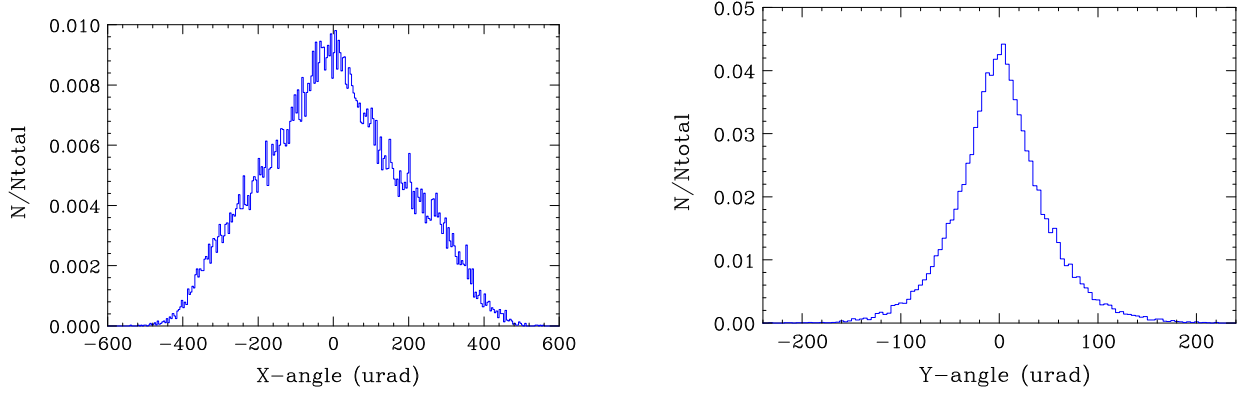


Figure 6: Beamstrahlung angular distribution (μrad) at IP with the TDR parameters for $3.6 \cdot 10^4$ photons.

The quadrupole focusing in the beginning of the line is designed to provide a secondary focal point with an optimal transformation for polarization measurement, and large chromatic and geometric acceptance for the electron and photon beams. Downstream of the quadrupoles, the optics includes six vertical dipoles providing conditions for measurements of beam energy, polarization and luminosity [8]. After the last dipole, there are 5 horizontal and 5 vertical fast sweeping kickers which function is to increase the effective beam area at the dump for protecting the dump window from high beam power density and preventing water boiling in the dump. The extraction collimation system includes two protection collimators within the dipole region and three collimators within the final 100 m before the dump. The latter protect the sweeping kickers and limit beam area to within 15 cm radius at the dump window.

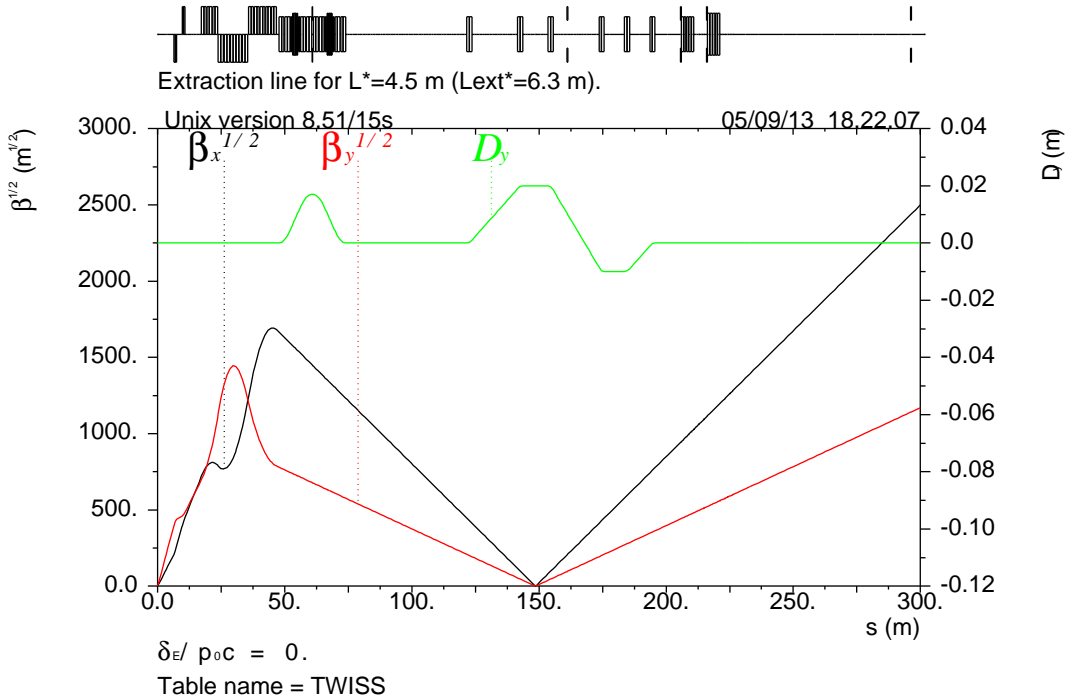


Figure 7: Extraction line layout (top) and optics functions with the TDR parameters.

As noted earlier, the disruption significantly changes the electron beam distribution. Consequently, this modifies the IP optics functions which can be computed from the statistical electron distribution generated by Guinea-Pig. The β and α functions at IP before and after disruption are shown in Table 4.

Table 4: Optics functions at IP for disrupted and undisrupted electron beam at IP with the TDR parameters.

IP beam	β_x^*	α_x^*	β_y^*	α_y^*
undisrupted	11 mm	0	0.48 mm	0
disrupted	3.29 mm	1.609	0.294 mm	0.386

Finally, a 5 T detector solenoid based on a silicon detector design (SiD) [9] is included in the tracking study. The orbit distortions due to the solenoid are compensated using dipole corrector windings in the superconducting (SC) extraction quadrupoles [2]. Additionally, a detector integrated dipole coil (anti-DiD) built on top of the solenoid is included as it helps minimizing the detector background [10].

4 Disrupted electron beam losses for the TDR parameters without detector solenoid

The extraction beam losses occur when electrons have either low energy or large x or y angles at IP. The tracking simulations show that in order to determine the complete losses, it is sufficient to track only the beam tail where energy is below 70% of the nominal energy or IP x or y angles are larger than 0.5 mrad (this accounts for $\approx 1.3\%$ electrons of the total beam with the TDR parameters). Only 52289 particles out of the high statistics beam of $4 \cdot 10^6$ particles satisfy the mentioned criteria. The resulting beam losses without the detector solenoid amounted to 5062 electrons. Fig. 8 shows the initial distribution of $\Delta E/E$ and horizontal angles at IP in the tracked beam tail, and distribution of electrons lost in the extraction line. One can see that, indeed, the lost electrons belong to the energy and angular tail as specified above. Note also the missing beam core in Fig. 8 which was not tracked for speeding up the calculation. Fig. 9 shows the initial and lost electron energy distribution for the full beam, without the solenoid.

Based on the electron loss data, one can obtain power losses in the extraction magnets, diagnostics and collimators as shown in Fig. 10. Most power losses occur in the collimators designed to protect the magnets and diagnostics as well as to control the beam spread at the dump. In this case, no loss was observed at the SC quadrupoles, and the losses in warm magnets are below 0.5 W/m which is acceptable. The maximum power loss in a collimator is 2.5 kW which is acceptable.

5 Disrupted electron beam losses for the TDR parameters with SiD detector solenoid

Similarly, the electron beam losses with the TDR parameters were calculated including the SiD detector solenoid and the anti-DiD dipole field. In this case, due to the crossing angle, the solenoid generates vertical orbit and dispersion as well as coupling to the beam. It is also assumed that the incoming orbit at IP has a non-zero vertical angle due to the effect of the upstream part of the solenoid. A conservatively large angle value of $y' = 100 \mu\text{rad}$ is used in the tracking.

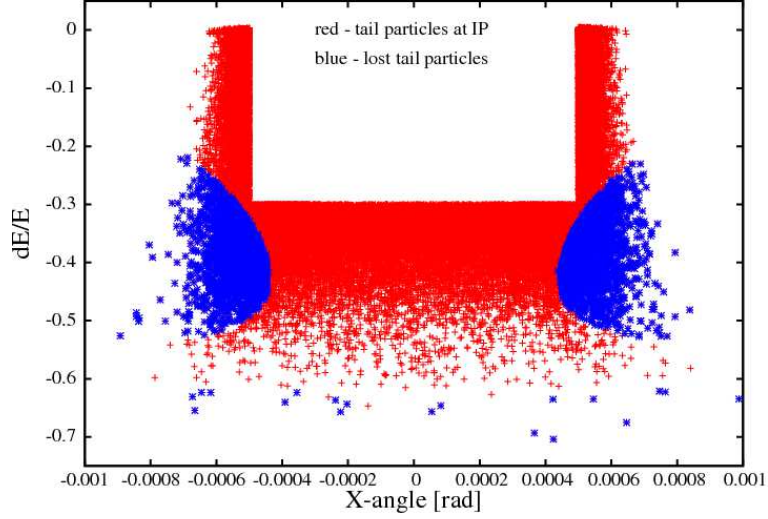


Figure 8: Initial energy and angular distribution of tail electrons with $E < 0.7 E_0$ or x or y angles > 0.5 mrad at IP (red), and distribution of lost electrons in the extraction line (blue) with the TDR parameters without detector solenoid.

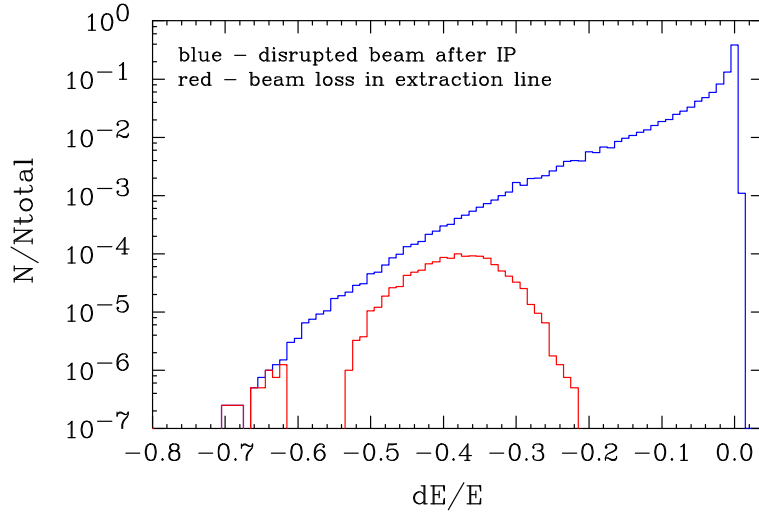


Figure 9: Initial disrupted electron energy distribution (blue), and distribution of lost electrons in the extraction line (red) with the TDR parameters without detector solenoid.

The first order orbit from the solenoid is locally corrected by the four dipole corrector windings included in the SC quadrupoles. However, the remaining residual chromatic and coupling distortion can increase the beam loss. The beam tail distribution at IP, as in the case without solenoid, was used in tracking with the SiD solenoid. The resulting energy and angular distributions of the initial and lost electrons are shown in Fig. 11 and 12. One can see that most electrons with low energy, regardless of initial $x - y$ angles, are lost. This effect is likely due to residual dispersion from the solenoid. The total electron losses are increased by a factor of 2 compared to the case without solenoid. These additional losses can be reduced if the incoming vertical angle at IP is compensated.

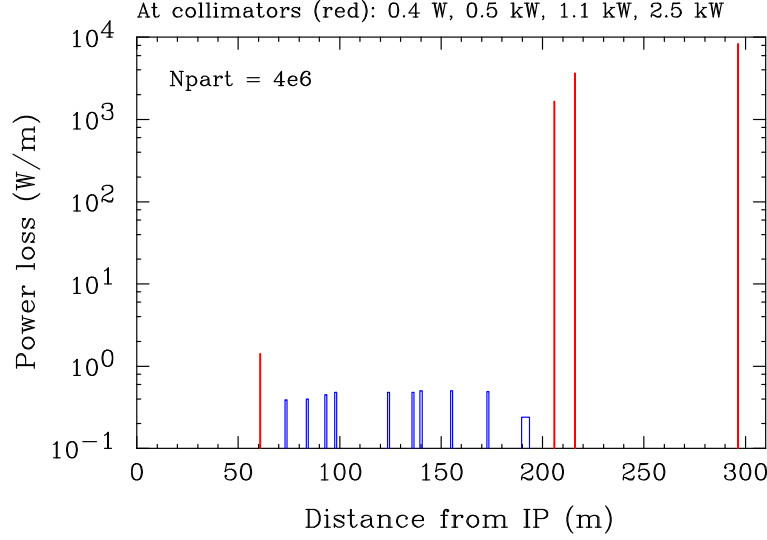


Figure 10: Power losses of the disrupted electron beam in the extraction line magnets and diagnostics (blue), and collimators (red) with the TDR parameters without detector solenoid.

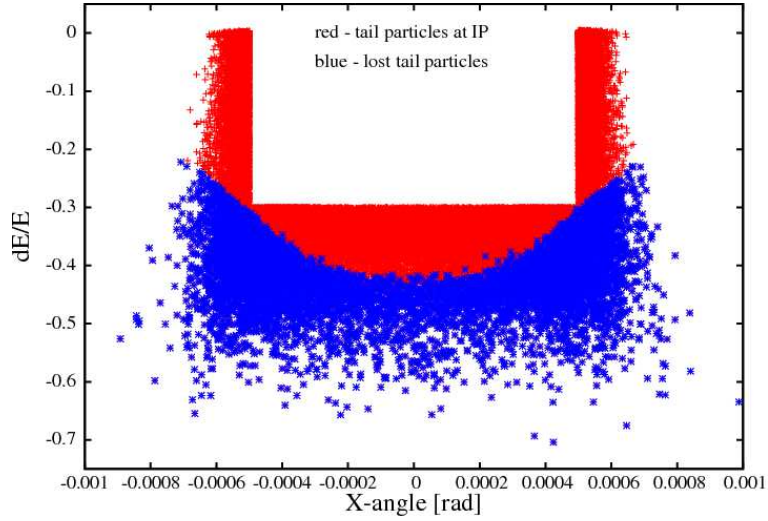


Figure 11: Initial energy and angular distribution of tail electrons with $E < 0.7 E_0$ or x or y angles > 0.5 mrad at IP (red), and distribution of lost electrons in the extraction line (blue) with the TDR parameters and SiD detector solenoid.

The electron power losses with the TDR parameters and the SiD solenoid are shown in Fig. 13. Most of the losses occur in the protection collimators due to their tighter apertures. No loss was observed in the SC quadrupoles, and losses in the warm magnets are below 12 W/m which should be acceptable. The maximum power loss in a collimator is 3 kW which is acceptable.

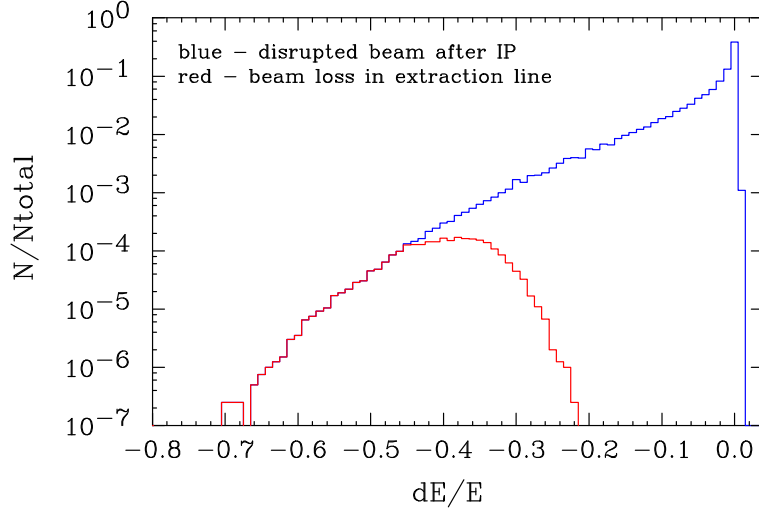


Figure 12: Initial disrupted electron energy distribution (blue), and distribution of lost electrons in the extraction line (red) with the TDR parameters and SiD detector solenoid.

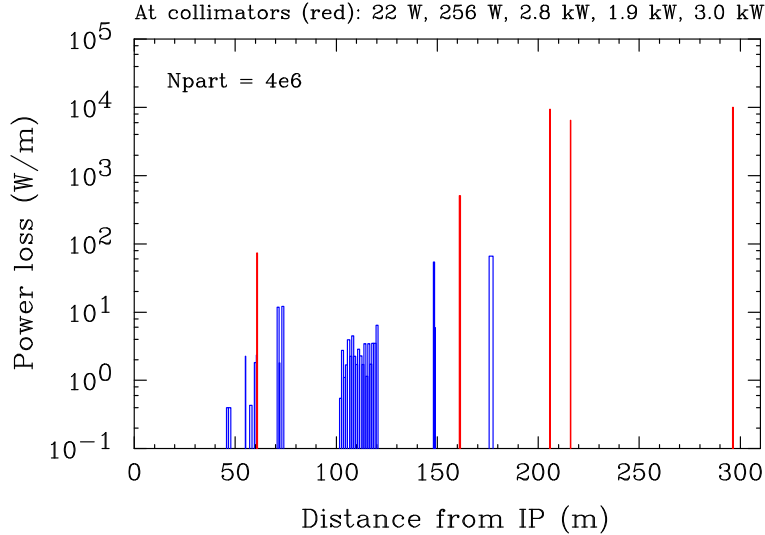


Figure 13: Power losses of the disrupted electron beam in the extraction line magnets and diagnostics (blue), and collimators (red) with the TDR parameters and SiD detector solenoid.

6 Electron beam power losses in the RDR nominal and low-P options with SiD detector solenoid

For comparison, the electron beam power losses were also calculated for the RDR nominal and low-P options, including the SiD detector solenoid and the anti-DiD dipole coil field. In the nominal option, the tracking was performed using a beam tail extracted from $3.5 \cdot 10^7$ beam data. In case of the low-P parameters, where disruption is much stronger, the tracking was done with a full beam containing $7 \cdot 10^4$ particles. The same incoming vertical angle of $100 \mu\text{rad}$ at IP was used as in the TDR tracking.

Power losses in the RDR nominal and low-P options are shown in Fig. 14 and 15. The losses

in the nominal option are lower compared to the TDR case due to smaller disruption resulting in a shorter low energy tail.

The losses in the low-P option are significantly higher compared to both the TDR and RDR nominal options due to higher disruption. Although there is no loss in the SC quadrupoles, the power losses in warm magnets are up to 130 W/m, and there are rather high losses in the diagnostic detectors (at $S \approx 150$ m and 175 m) which may be a concern. The maximum power loss at a collimator is 14.8 kW which can be acceptable with a proper design.

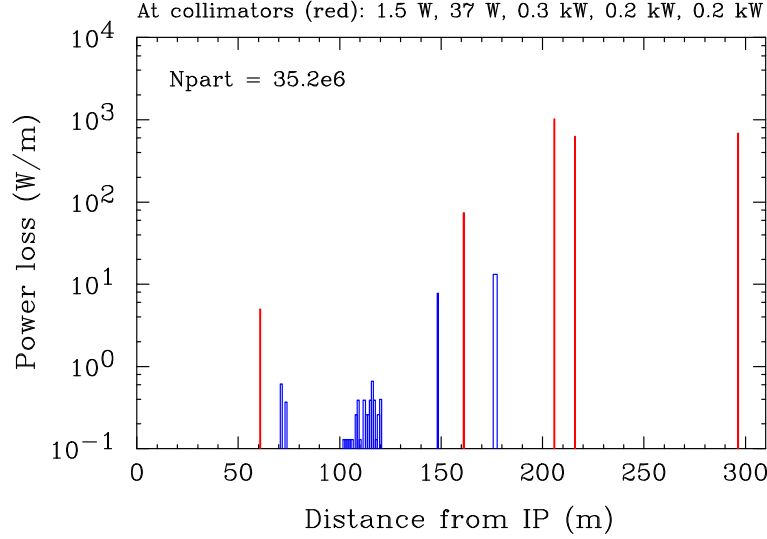


Figure 14: Power losses of the disrupted electron beam in the extraction line magnets and diagnostics (blue), and collimators (red) with the SiD detector solenoid and RDR nominal parameter option.

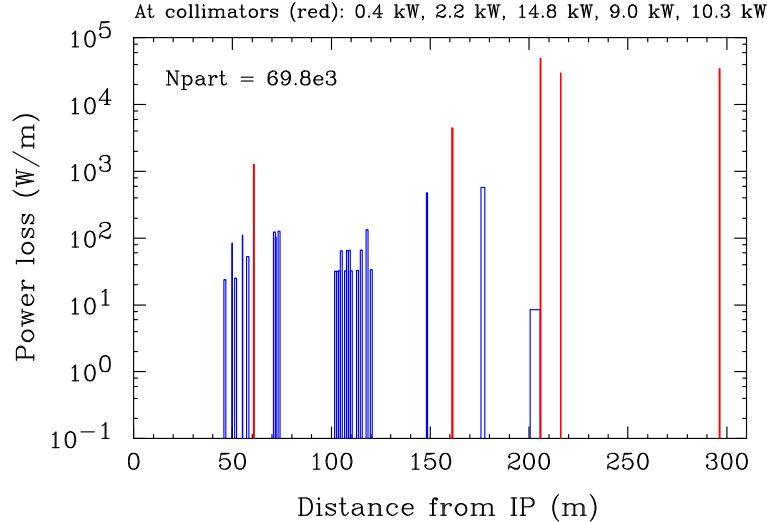


Figure 15: Power losses of the disrupted electron beam in the extraction line magnets and diagnostics (blue), and collimators (red) with the SiD detector solenoid and RDR low-P parameter option.

7 Beamstrahlung photon power losses with the TDR parameters

Since the photon trajectories are not affected by magnetic field, their losses are determined only by their $x - y$ angles at IP and the extraction aperture. By design, the extraction aperture accepts the IP photon angles up to ± 0.75 mrad within the magnets and diagnostics ($S = 0$ to 200 m), and ± 0.5 mrad in the dump collimators ($S = 200$ to 300 m). Tracking was performed for $3.6 \cdot 10^4$ beamstrahlung photons corresponding to $2 \cdot 10^4$ primary electrons. In agreement with the photon angular distribution in Fig. 6, where maximum angle is below 0.75 mrad, there were no photon losses in magnets and diagnostics. A rather small loss of 100 W occurred at two protection collimators about 90 m upstream of the dump.

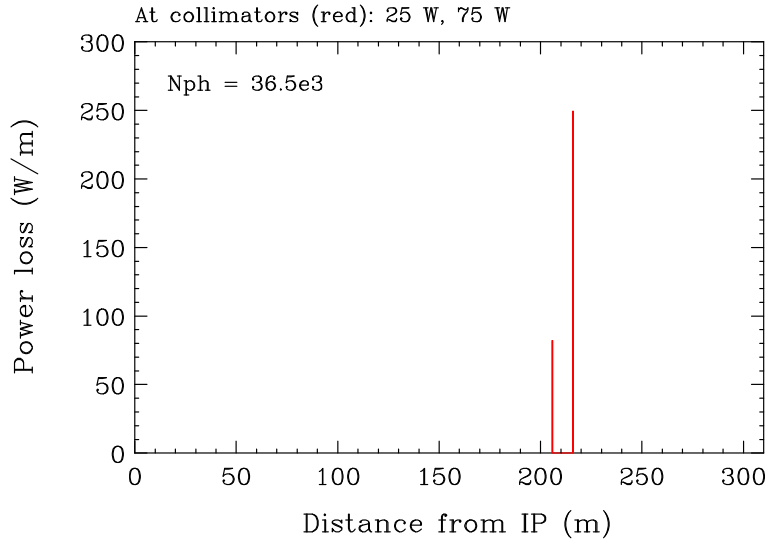


Figure 16: Power losses of beamstrahlung photons in the extraction line collimators with the TDR parameters. No losses occurred in magnets and diagnostics for $3.6 \cdot 10^4$ tracked photons.

8 Summary of extraction losses and conclusions

Table 5 summarizes electron power losses in magnets, diagnostic detectors and collimators for the TDR parameters and the RDR nominal and low-P options with the SiD detector solenoid. One can see that the power losses in extraction magnets with the TDR parameters are an order of magnitude higher than in the RDR nominal option, but an order of magnitude lower than in the RDR low-P option. Overall, the electron beam losses in the extraction magnets and collimators with the TDR parameters appear to be acceptable. Losses in the diagnostic detectors may need an expert opinion to evaluate the impact on the background signal. The beamstrahlung photon losses with the TDR parameters are rather small.

However, the presented calculations were done assuming ideal collision conditions. Non-ideal conditions, such as large vertical beam-to-beam separation at IP, will increase the beam disruption and, consequently, the extraction beam losses [11]. Evaluation of these effects requires a separate study.

Table 5: Summary of disrupted electron beam loss in the extraction line with the SiD detector solenoid for the TDR parameters and the RDR nominal and low-P options.

	Magnets		Diagnostic Detectors		Collimators				
	SC	Warm (max)	Synchrotron	Cherenkov	Energy chicane	Cherenkov	Dump 1	Dump 2	Dump 3
TDR	0	12 W/m	30 W	130 W	22 W	0.3 kW	2.8 kW	1.9 kW	3.0 kW
Nominal	0	0.6 W/m	4 W	26 W	2 W	37 W	0.3 kW	0.2 kW	0.2 kW
Low-P	0	130 W/m	0.5 kW	0.6 kW	0.4 kW	2.2 kW	14.8 kW	9.0 kW	10.3 kW

References

- [1] Y. Nosochkov, K. Moffeit, Andrei Seryi, W. Morse, B. Parker, “14 mrad Extraction Line Optics for Push-Pull”, SLAC-PUB-12856, LCWS-2007-MDI13 (2007).
- [2] D. Toprek, Y. Nosochkov, “Evaluation and Compensation of Detector Solenoid Effects on Disrupted Beam in the ILC 14 mrad Extraction Line”, Nucl. Instrum. Meth. A612, 260-273 (2010).
- [3] J. Brau (Ed.) *et al.*, ILC Reference Design Report, v.3, ILC-Report-2007-001 (2007).
- [4] T. Behnke (Ed.) *et al.*, ILC Technical Design Report 2013, v.3, <http://www.linearcollider.org/ILC/Publications/Technical-Design-Report>.
- [5] R.T. Garcia, <http://clcr.web.cern.ch/CLICr/ILC/>.
- [6] D. Schulte, “Study of Electromagnetic and Hadronic Background in the Interaction Region of the TESLA Collider”, PhD Thesis, TESLA-97-08 (1996).
- [7] <http://www.slac.stanford.edu/accel/ilc/codes/dimad/>.
- [8] K. Moffeit, T. Maruyama, Y. Nosochkov, A. Seryi, M. Woodley, M. Woods, “Proposal to Modify the Polarimeter Chicane in the ILC 14 mrad Extraction Line”, SLAC-PUB-12425 (2007).
- [9] T. Behnke (Ed.) *et al.*, ILC Technical Design Report 2013, v.4, <http://www.linearcollider.org/ILC/Publications/Technical-Design-Report>, and <http://www.silicondetector.org/display/SiD/home>.
- [10] A. Seryi, T. Maruyama, B. Parker, “IR Optimization, DID and anti-DID”, SLAC-PUB-11662 (2006).
- [11] Y. Nosochkov, T.O. Raubenheimer, K.A. Thompson, “NLC beam properties and extraction line performance with beam offset at IP”, SLAC-PUB-8872, PAC-2001-FPAH065 (2001).